Journal of Materials Chemistry

Dynamic Article Links

Cite this: J. Mater. Chem., 2011, 21, 18195

www.rsc.org/materials

COMMUNICATION

3D boron doped carbon nanorods/carbon-microfiber hybrid composites: synthesis and applications in a highly stable proton exchange membrane fuel cell†

Jiajun Wang,[a] Yougui Chen,[a] Yong Zhang,[a] Mihnea Ioan Ionescu,[a] Ruying Li,[a] Xueliang Sun,*[a] Siyu Ye[b] and Shanna Knights[b]

Received 6th August 2011, Accepted 5th October 2011
DOI: 10.1039/c1jm13796d

Boron-doped carbon nanorods (BCNRs) were directly grown on carbon-microfiber by the spray pyrolysis chemical vapour deposition method. The stability of the deposited Pt nanoparticles was found to be increased by more than three times with substitutional boron dopants in 3D carbon nanomaterials. Our work will be of great technological significance for developing highly stable electrode materials in fuel cells.

Currently, one of the major limitations to the commercialization of proton exchange membrane fuel cells (PEMFCs) is the material durability, especially the stability of the Pt/C electrocatalyst.[1] It is generally believed that widely used Vulcan XC-72 carbon support is susceptible to a serious corrosion process by surface oxidation and CO_2 evolution in PEMFC systems.[2] This process severely affects the stability of Pt catalyst through detachment from the support and accelerated coalescence of Pt nanoparticles on the support. It is known that the tendency of Pt nanoparticle coalescence may be reduced by increasing the interaction between Pt and its supports.[3] Therefore, a support with both high corrosion resistance and a strong metal–support interaction is highly desirable.

Recently, carbon nanotubes (CNTs) have been proposed as promising support materials for fuel cell catalysts due to their unique characteristics.[4] However, due to their inherit inert surface, CNTs have to be surface functionalized to provide anchoring sites for Pt nanoparticles. In general, acid treatment is used to introduce functional groups,[5] but it also destroys the intrinsic structure and properties of CNTs. A mild functionalization is therefore necessary without sacrificing the intrinsic structure and properties, particularly the electrochemical stability. Doping the CNTs with heteroatoms could offer a possible route for mild surface modification.[6] In our previous work, structural and morphological control in the nitrogen doped CNTs (N-CNTs) was investigated.[7] More recently, our results indicated that N-CNTs as Pt catalyst supports can enhance the electrochemical performance and significantly improve the catalyst's durability in PEMFCs.[8] Similarly, boron doping is also a novel strategy. The presence of substitution boron defects can significantly increase the adsorption energies of nano-metal clusters compared to the pristine carbon material.[9] A superior electrochemical performance has been reported using diamond powder doped with boron for fuel cell applications.[10] Thus, a stable Pt catalyst may be expected if using boron doped carbon nanomaterials as catalyst supports.

Here, for the first time, we present novel boron doped carbon nanorods (BCNRs) directly grown on carbon paper as a 3D hybrid composite electrode for PEMFCs. A 3D electrode structure built by direct growth of one-dimensional nanostructures on carbon microfibers based on carbon paper has shown high performance for PEMFCs.[11] We demonstrated here that Pt deposited on this new material shows high activity for oxygen reduction reaction (ORR). Most importantly, the 3D BCNR electrodes demonstrated significantly improved durability of the Pt catalyst by over three times compared with CNTs, which might be of great technological significance for PEMFCs.

CNTs and BCNRs were grown on the carbon papers by the spray pyrolysis chemical vapour deposition method (Fig. S1 and S2, ESI†), and the scanning electron microscope (SEM) images are shown in Fig. 1. As shown in Fig. 1a and b, CNTs with a high density uniformly covering the carbon fibers exhibit a high degree of alignment. The aligned CNTs have an average length of 3 μm and the diameter ranges from 20 to 50 nm. With the introduction of boron (Fig. 1c and d), carbon nanomaterials with a significantly short length (to only ~10% of the length of the CNTs) have been obtained. It is obvious that the introduction of boron severely inhibits the growth of carbon nanomaterial as revealed from the decreased diameter and length. The inhibition effect may be attributed to the slow carbon bulk diffusion in the presence of boron which is similar to nitrogen-mediated carbon nanotube growth in diameter reduction and length shortness.[12] In addition, the high oxygen content contained in the boron source (B_2O_3) may also induce the oxidation of graphite and reduce the growth of carbon nanomaterial. Fig. 1(e)–(g) show the morphologies of BCNRs during the growth process (2, 5, 20 min).

[a]*Department of Mechanical and Materials Engineering, University of Western Ontario, London, Ontario, Canada N6A 5B9. E-mail: xsun@eng.uwo.ca*
[b]*Ballard Power Systems Inc., 9000 Glenlyon Parkway, Burnaby, BC, Canada V5J 5J8*

† Electronic supplementary information (ESI) available: Experimental section, additional schematic figure of the spray CVD apparatus, digital photograph, EELS mapping, XPS of BCNR, and TEM images of Pt nanoparticles on a CNT and a BCNR before and after the fuel cell durability test. See DOI: 10.1039/c1jm13796d

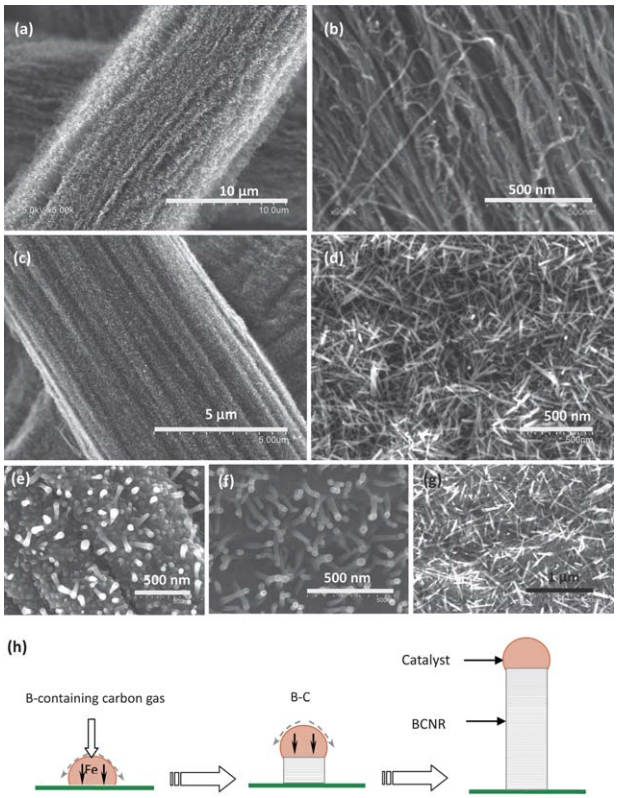

Fig. 1 SEM images of CNTs (a and b) and BCNRs (c and d) grown on carbon papers at different magnifications. SEM images illustrating the growth process of BCNRs at (e) 2 min, (f) 5 min, (g) 20 min and the corresponding schematic diagram (h).

The spherical iron catalyst, from ferrocene, used to grow the BCNRs was located at the tip of each BCNR. We therefore propose that the BCNRs grow *via* a tip-growth mechanism.[13a] During the carbon nanomaterial growth process, there are two diffusion paths of the decomposed carbon on the catalyst, bulk diffusion path (the black arrows) and surface diffusion path (the dashed arrows).[13b] The schematic diagram illustrates the growth process of BCNRs. With the introduction of boron, the bulk diffusion is predominant and the decomposed carbon penetrates through the catalyst particle much faster than its saturation on the catalyst surface, thus precipitates at the catalyst–substrate interface to form BCNRs.

Acid treatment and washing were carried out to remove the iron catalysts and remaining B_2O_3 impurities in the BCNRs. Transmission electron microscopy (TEM) was performed on the clean BCNR sample and the images are shown in Fig. 2. BCNRs show a uniform length and diameter. The selected area electron diffraction (SAED) pattern depicts various diffraction rings, which can be indexed as the crystal planes of graphitic carbon (inset in Fig. 2a). In the HRTEM image in Fig. 2b, there is no inner hollow found in the BCNRs, confirming that the BCNR is a nanorod (or nanofibre) structure but not nanotubes. The interplanar spacing of (100) in BCNRs is 2.25 Å, which is higher than the reference value of carbon (100) (2.1391 Å, PDF#75-1621). It is evident that boron doping expands a carbon lattice structure relative to undoped carbon nanotubes.

The elemental components and distributions were further analyzed by EELS. Fig. 2c shows the EELS recorded over a random BCNR bundle region. The corresponding spectra displays two absorption

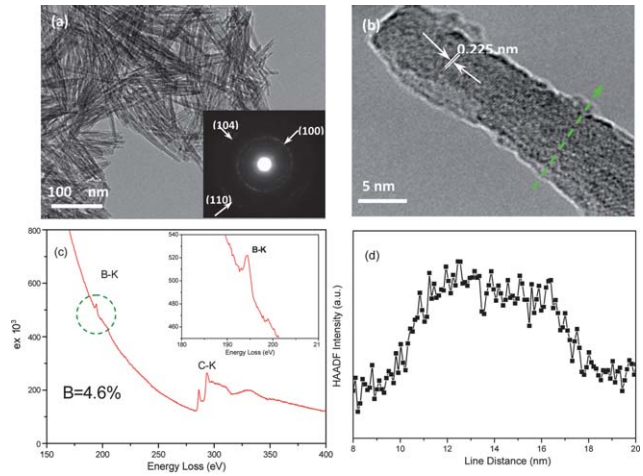

Fig. 2 (a) HRTEM images of BCNR bundles and selected area electron diffraction; (b) HRTEM images of an individual BCNR; (c) EELS recorded at BCNR bundles; (d) B intensity profile in a line scan indicated in image of Fig. 3(b).

edges, a strong C–K edge at about 285 eV and a weak B–K edge at about 190 eV, respectively. The boron content in these BCNR bundles is determined to be 4.6 at.%, slightly lower than that found in the XPS result (4.9 at.%, Fig. S3, ESI†), which can be due to the removal of the remaining B_2O_3 impurity in the acid treatment and washing process. The EELS line-scan across an individual nanorod was performed (Fig. 2d), and boron is found to be homogenously distributed within the nanorod structure. The intensity range of the B signal is around 7 nm, corresponding to the diameter for individual BCNRs. The homogeneity of the B distribution in the BCNRs was further confirmed by the EELS mapping performed at a randomly selected BCNR bundle region (Fig. S4, ESI†). Here it should be mentioned that a small amount of iron element was also found in XPS result, as bright points shown on the surface/inside of nanotubes and the tips of nanorodes in Fig. 1. However, most of these iron elements will be removed and fewer iron particles remain on the carbon nanomaterials after the acid purification and washing process (Fig. 2a).[6,14a] Even if some negligible iron remains inside the carbon nanomaterials, it has no obvious effects on the following electrochemical performance test because it was reported that there was no apparent correlation between the presence of an iron phase and activity.[14b] This iron-catalyzed growth of carbon nanomaterials and the similar purification process have been widely reported for PEMFC application in numerous studies.[14]

The comparative durability investigation of the Pt nanoparticles deposited on the corresponding supports for a PEMFC was performed by an accelerated durability test (ADT). Fig. 3a and c show the representative cyclic voltammograms (CV) of Pt/BCNRs and Pt/CNTs before and after 3000 ADT cycles. It can be seen that a reduction in the hydrogen adsorption and desorption in the CV appeared on both catalysts with the potential cycling, which shows a decrease in the electrochemical surface area (ECSA) for each catalyst. The calculated result reveals that the ECSA of the Pt/BCNR electrode (Fig. 3e and g) decreases from 68.2 to 32.5 $m^2\ g^{-1}$ after ADT cycles, 47.7% of its initial ECSA still remained (Table 1). It is remarkably larger than that for Pt/CNTs, for which only 13.2% of its initial ECSA remained. This result indicates that the Pt/BCNR

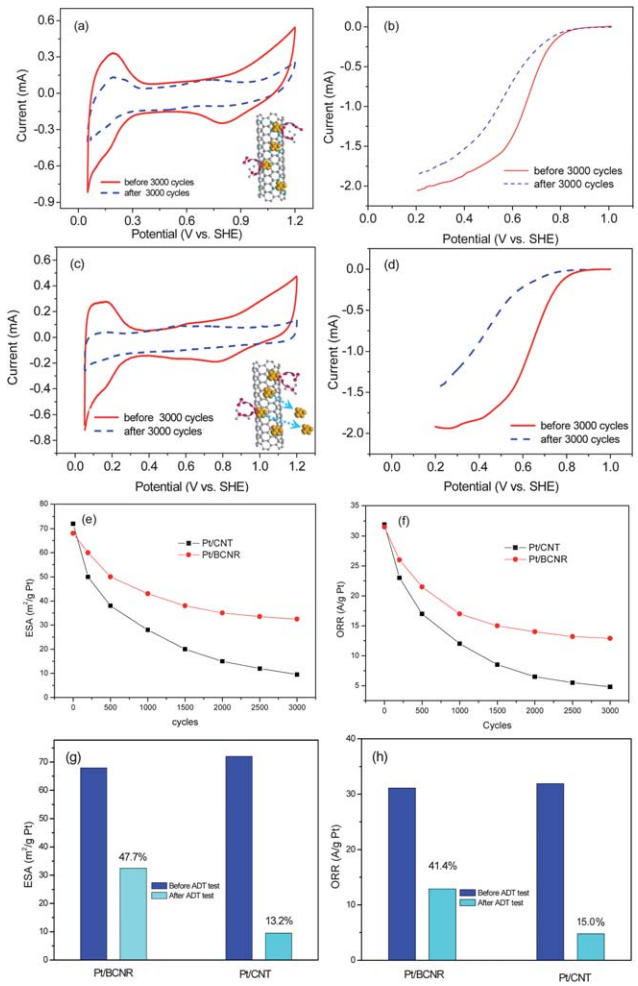

Fig. 3 Comparison of electrochemical stability of Pt/BCNRs and Pt/CNTs tested in 0.5 M H_2SO_4 solution. Cyclic voltammograms (a) and oxygen reduction polarization curves (b) of Pt/BCNRs before and after ADT; cyclic voltammograms (c) and oxygen reduction polarization curves (d) of Pt/CNTs before and after ADT; the ESA (e) and ORR activity (f) as a function of cycle number for the two electrodes; the histogram comparison of the ECSA (g) and ORR activity (h) before and after ADT.

electrode has over three times higher stability than Pt/CNTs. Fig. 3b and d show the representative ORR curves of Pt/BCNR and Pt/CNT catalysts before and after ADT cycles. Both catalysts exhibit an obvious negative shift of the potentials in the ORR curves after the ADT, which means a decrease in ORR activity on the catalysts. Compared to Pt/CNTs, Pt/BCNRs showed less potential shift toward the negative direction. The half-wave potential ($E_{1/2}$) for Pt/BCNRs shows only an 80 mV change after 3000 ADT cycles, while it is 190 mV for Pt/CNTs. This suggests a higher stability of Pt/BCNRs during the ORR. A further comparison of ORR activity was carried out based on the kinetic current density at 0.85 V, which is shown in Fig. 3f and h. Although a decrease in kinetic current density for Pt/BCNRs is observed, it still shows a higher value of 12.9 A g^{-1} Pt, *i.e.* 41.4% of its initial value (31.2 A g^{-1} Pt). In comparison, the Pt/CNT catalyst retained only 15.0% of the initial value.

After ADT, large amounts of Pt nanoparticles were lost on the CNT support (ESI, Fig. S5†). In contrast, the Pt/BCNRs show less Pt

Table 1 Pt loadings, ESA and ORR activity for Pt/BCNR and Pt/CNT electrode before and after ADT test

Catalysts	Pt loadings/ μg cm^{-2}	ESA/m^2 g^{-1} Pt		ORR activity (@0.85 V)/ A g^{-1} Pt	
		Before ADT	After ADT	Before ADT	After ADT
Pt/BCNR	58	68.2	32.5	31.2	12.9
Pt/CNT	60	72.0	9.5	31.9	4.8

detachment from the support, indicating a stronger bonding energy between Pt nanoparticle and BCNR supports. It has been shown using first-principles density functional theory calculations that the adsorption energies of the Pt clusters increase significantly in the presence of boron in carbon supports.[15a] The enhanced Pt adsorption at B doped carbon nanomaterial can be attributed to a strong hybridization between the Pt *d* orbital and B *p* orbital, leading to direct chemical bonding between Pt and B atoms.[9,15b] In addition, the reduced sintering of the Pt/BCNR catalyst may also be attributed to the increasing corrosion resistance of the BCNR support. During the corrosion process of BCNRs, oxygen preferentially attacks boron atom,[15c] forming boron oxides (one of the reasons for high oxygen content in as-prepared BCNRs, XPS spectra in Fig. S3 in the ESI†). It could thus have an inhibiting effect on carbon corrosion. Meanwhile, the formed boron oxides will passivate the carbon surface, thus further inhibiting carbon corrosion and improving the stability of Pt/BCNRs. Besides, the 3D electrode structure might contribute to the high stability through a lower possibility of Pt nanoparticle agglomeration than those non-3D electrodes, but this might not be the main reason for the higher stability of Pt/BCNRs compared with Pt/CNTs because both electrodes here are 3D structured.

In conclusion, for the first time, we successfully synthesized 3D boron-doped carbon nanorods (4.6 at.% boron element) directly grown on the carbon paper. This new nanocomposite, when used as the catalyst support, significantly improves the Pt nanoparticle stability. ADT results indicated that the enhanced stability of Pt nanoparticles was achieved on the BCNR support, which could be attributed to the strong and direct chemical bonding between Pt and B atoms, the high corrosion resistance of BCNRs itself, and possibly the 3D electrode structure. Our BCNR electrode can be used not only as a promising catalyst support for fuel cells, but also as a novel nanomaterial for various energy and environmental applications.

Acknowledgements

This work is supported by Natural Sciences and Engineering Research Council of Canada (NSERC), Ballard Power Systems, Canada Research Chair (CRC) Program, MITACS Elevate Strategic Fellowship Program, and the University of Western Ontario.

Notes and references

1 (*a*) R. Borup, J. Meyers, B. Pivovar, Y. S. Kim, R. Mukundan, N. Garland, D. Myers, M. Wilson, F. Garzon, D. Wood, P. Zelenay, K. More, K. Stroh, T. Zawodzinski, J. Boncella, J. E. McGrath, M. Inaba, K. Miyatake, M. Hori, K. Ota, Z. Ogumi, S. Miyata, A. Nishikata, Z. Siroma, Y. Uchimoto, K. Yasuda, K.-I. Kimijima and N. Iwashita, *Chem. Rev.*, 2007, **107**, 3904–3951; (*b*) X. Yu and S. Ye, *J. Power Sources*, 2007, **172**, 145–154.

2 J. J. Wang, G. P. Yin, Y. Y. Shao, S. Zhang, Z. B. Wang and Y. Z. Gao, *J. Power Sources*, 2007, **171**, 331–339.
3 J. Zhou, X. Zhou, X. Sun, R. Li, M. Murphy, Z. Ding, X. Sun and T.-K. Sham, *Chem. Phys. Lett.*, 2007, **437**, 229–232.
4 (*a*) H. Chu, Y. Shen, L. Lin, X. Qin, G. Feng, Z. Lin, J. Wang, H. Liu and Y. Li, *Adv. Funct. Mater.*, 2010, **20**, 3747–3752; (*b*) M. Saha, R. Li and X. Sun, *J. Power Sources*, 2008, **177**, 314–322; (*c*) J. J. Wang, G. P. Yin, Y. Y. Shao, Z. B. Wang and Y. Z. Gao, *J. Phys. Chem. C*, 2008, **112**, 5784–5789.
5 J. J. Wang, G. P. Yin, Y. Y. Shao, Z. B. Wang and Y. Z. Gao, *J. Electrochem. Soc.*, 2007, **154**, B687–B693.
6 K. Gong, F. Du, Z. Xia, M. Durstock and L. Dai, *Science*, 2009, **323**, 760–764.
7 H. Liu, Y. Zhang, R. Y. Li, X. L. Sun, S. Desilets, H. Abou-Rachid, M. Jaidann and L. S. Lussier, *Carbon*, 2010, **48**, 1498–1507.
8 (*a*) M. Saha, R. Y. Li, X. L. Sun and S. Y. Ye, *Electrochem. Commun.*, 2009, **11**, 438–441; (*b*) Y. G. Chen, J. J. Wang, H. Liu, Y. R. Li, X. L. Sun, S. Y. Ye and S. Knights, *Electrochem. Commun.*, 2009, **11**, 2071–2076.
9 Y. H. Li, T. H. Hung and C. W. Chen, *Carbon*, 2009, **47**, 850–855.
10 G. R. Salazar-Banda, K. I. B. Eguiluz and L. A. Avaca, *Electrochem. Commun.*, 2007, **9**, 59–64.
11 (*a*) X. Sun, R. Li, D. Villers, J. P. Dodelet and S. Desilets, *Chem. Phys. Lett.*, 2003, **379**, 99–104; (*b*) J. J. Wang, G. P. Yin, Y. G. Chen, R. Y. Li and X. L. Sun, *Int. J. Hydrogen Energy*, 2009, **34**, 8270–8275.
12 B. G. Sumpter, V. Meuniert, J. M. Romo-Herrera, E. Cruz-Silva, D. A. Cullen, H. Terrones, D. J. Smith and M. Terrones, *ACS Nano*, 2007, **1**, 369–375.
13 (*a*) X. Tao, L. Dong, X. Wang, W. Zhang, B. J. Nelson and X. Li, *Adv. Mater.*, 2010, **22**, 2055–2059; (*b*) R. H. Baughman, A. A. Zakhidov and W. A. deHeer, *Science*, 2002, **297**, 787–792.
14 (*a*) W. Li, C. Liang, W. Zhou, J. Qiu, Z. Zhou, G. Sun and Q. Xin, *J. Phys. Chem. B*, 2003, **107**, 6292–6299; (*b*) P. H. Mattrer, E. Wang, J.-M. M. Millet and U. S. Ozkan, *J. Phys. Chem. C*, 2007, **111**, 1444–1450; (*c*) R. H. Baughman, A. A. Zakhidoc and W. A. deHeer, *Science*, 2002, **297**, 787–792.
15 (*a*) C. K. Acharya and C. Heath Turner, *J. Phys. Chem. B*, 2006, **110**, 17706–17710; (*b*) W. An and C. Heath Turner, *J. Phys. Chem. C*, 2009, **113**, 7069–7078; (*c*) C. K. Acharya, W. Li, Z. Liu, G. Kwon, C. Heath Turner, A. M. Lane, D. Nikles, T. Klein and M. Weaver, *J. Power Sources*, 2009, **192**, 324–329.

